Mater. Res. Soc. Symp. Proc. Vol. 898E © 2006 Materials Research Society 0898-L09-04.1

Fatigue Microdamage in Bovine Cortical Bone Imaged by Micro-Computed Tomography Using a Barium Sulfate Contrast Agent

Huijie Leng, Xiang Wang, Glen L. Niebur and Ryan K. Roeder
Department of Aerospace and Mechanical Engineering, University of Notre Dame
Notre Dame, IN 46556, U.S.A.

ABSTRACT

Accumulation of microdamage during fatigue can lead to increased fracture susceptibility in bone. Current techniques for imaging microdamage in bone are inherently destructive and two-dimensional. A non-destructive, three-dimensional technique is needed to measure the spatial density of microdamage accumulation. Therefore, the objective of this study was to image microdamage accumulation in cortical bone during fatigue using micro-computed tomography (micro-CT) with a barium sulfate ($BaSO_4$) contrast agent. Bovine cortical bone beams were loaded under four-point bending fatigue. Two symmetric notches were machined on the tensile surface in order to generate damage at the stress concentrations during loading. Specimens were loaded to a specified number of cycles or until one notch fractured, such that the other notch exhibited accumulated microdamage just prior to fracture. Microdamage ahead of the notch was stained by precipitation of $BaSO_4$ and imaged using micro-CT. Reconstructed images showed a distinct region of bright voxels around the notch tip or along propagating cracks due to the presence of $BaSO_4$, which was verified by backscattered electron imaging and energy dispersive spectroscopy. The stained region exhibited a characteristic kidney shape perpendicular to the notch tip, which was correlated to principal strain contours calculated by finite element analysis. The area of stained regions was positively correlated with the number of loading cycles.

INTRODUCTION

Healthy bone is crucial to overall human health. Bone provides structural support for the body; protects soft tissues and organs; produces red blood cells; stores minerals; and transmits muscular forces during movement [1]. Microdamage accumulates in cortical bone *in vivo* due to repetitive loading and is observed in the form of microcracks or diffuse damage [2,3]. *In vitro* studies have shown that microdamage accumulation has a detrimental effect on the mechanical properties of cortical bone [4,5]. However, *in vivo*, microdamage is repaired by, and may signal, bone remodeling [6-8]. Thus, excessive accumulation of microdamage prior to remodeling can lead to increased fracture susceptibility. However, the mechanistic role of microdamage in bone fragility is not yet well understood, in part, due to our limited capabilities for imaging and measuring microdamage accumulation.

Current techniques, such as UV or light microscopy using fluorescent stains [9-12], backscattered electron imaging (BEI) using a lead-uranyl acetate stain [13], laser scanning confocal microscopy (LSCM) using fluorescent stains [14,15] and serial imaging using fluorescent stains [15], require the preparation of many histologic sections which are inherently destructive and two-dimensional. A non-destructive and three-dimensional (3D) technique would enable researchers to measure the spatial density of microdamage accumulation, which could be correlated to local variations in mechanical loading, bone mineral density (BMD) or microarchitecture. Therefore, researchers are currently investigating noninvasive, 3D imaging techniques. Positron emission tomography (PET) was used to image microdamage *in vivo* using a sodium fluoride ($Na^{18}F$) contrast agent [16]. Micro-computed tomography (micro-CT) was

used to detect microdamage with a lead sulfide (PbS) contrast agent in cortical bone [17] and a barium sulfate ($BaSO_4$) contrast agent in trabecular bone [18].

The objective of this study was to nondestructively and three-dimensionally image microdamage accumulation in cortical bone using micro-CT with a $BaSO_4$ contrast agent. $BaSO_4$ was chosen as the contrast agent to label damage for micro-CT due to its biocompatibility and high x-ray attenuation. Microdamage was induced in bovine cortical bone beams by four-point bending fatigue. Two symmetric notches were created on the tensile surface in order to generate damage around the stress concentrations during loading. The double-notched beams enabled the study of microdamage in bone just prior to fracture [19-21].

EXPERIMENTAL METHODS

Twenty-four parallelepiped beams, 4 x 4 x 50-60 mm, were sectioned from the cortex at the mid-diaphysis of bovine tibiae. On the tensile surface of each beam, two symmetric notches were machined 10 mm apart to a depth of 1.2 mm and width of 300 μm using a low speed diamond saw (Fig. 1). Specimens were randomly divided into six groups which were loaded in four-point bending fatigue to 0 (unloaded control), 10^5, $2{\cdot}10^5$, $3{\cdot}10^5$, $4{\cdot}10^5$ and $5{\cdot}10^5$ cycles under displacement control (0.1 to 0.3 mm) at a frequency of 2 Hz, while soaking in de-ionized (DI) water under ambient conditions. Loading was stopped after reaching the designated number of cycles or when fracture occurred. Specimens that fractured prior to the designated number of cycles were reassigned to the appropriate group based on the number of cycles to failure.

After mechanical loading, all specimens were sectioned at the midspan (Fig. 1). Specimen halves with notches that did not fracture were stained by $BaSO_4$ precipitation, soaking in an equal parts mixture of 1 M barium chloride (Certified ACS crystal, Fisher Scientific) in DI water, buffered saline and acetone for 7 d, followed by an equal parts mixture of 1 M sodium sulfate (Anhydrous powder, Fisher Scientific) in DI water, buffered saline and acetone for 7 d, both under vacuum. Barium chloride and sodium sulfate solutions were neutralized by sodium hydroxide (ACS reagent, Sigma Chemical) and nitric acid (ACS reagent, Aldrich Chemical).

Specimens stained by $BaSO_4$ were imaged using micro-CT (μCT-80, Scanco Medical AG) at 10 μm resolution, 70 kVp voltage and 113 μA current with slices taken either transversely or longitudinally. For transverse slices, a 1.6 mm long region was scanned using a 200 ms integration time, which fully spanned the unbroken notch. Longitudinal slices were imaged to a depth of 0.8 mm using a 300 ms integration time. Gaussian smoothing was applied to images in order to suppress noise and 3D images were thresholded in order to show the $BaSO_4$ stain. After the background was removed, the intensity histogram was fit by the sum of two Gaussian curves (Fig. 2). The amount of stain in specimens was measured as the ratio of the $BaSO_4$ integrated peak intensity to the total integrated peak intensity. Linear regression was used to correlate the $BaSO_4$ integrated peak intensity to the number of loading cycles (JMP 5.1, SAS Institute, Inc.). The level of significance was 0.05. Specimens with macroscopic cracks propagating from the notch were not included in the regression.

Selected specimens were imaged using backscattered electron imaging (BEI) with a scanning electron microscope (SEM) (Evo 50, LEO Electron Microscopy, Inc.) at an accelerating voltage of 20 kV and a working distance of 7 mm. The elemental composition was measured by electron probe microanalysis (EPMA) using an energy dispersive spectrometer (EDS) (INCA x-sight model 7636, Oxford Instruments America). Specimens were embedded, sectioned, polished to a 0.25 μm final finish, washed with methanol, dried overnight in an oven at 90ºC and coated with gold by sputter deposition.

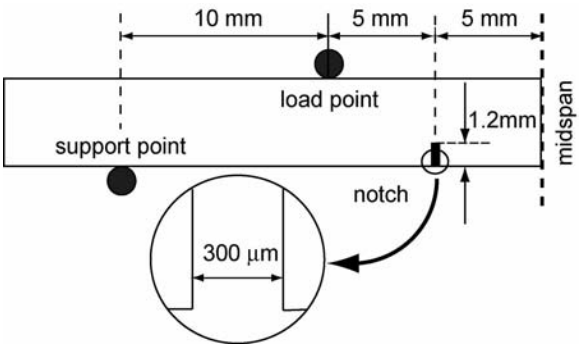

Figure 1. Schematic diagram of a double-notched four-point bending specimen, sectioned at the midspan.

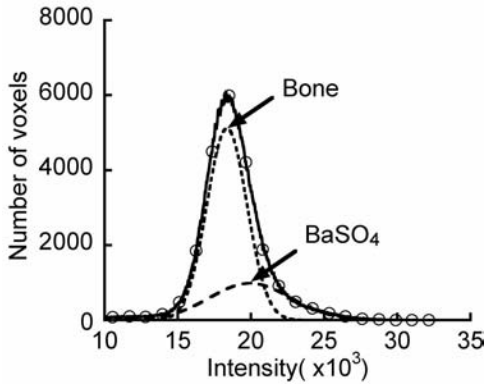

Figure 2. Micro-CT image intensity histogram fit using a two-peaked Gaussian function, showing bone and $BaSO_4$ peaks.

Finite element analysis (FEA) was used to qualitatively compare principal strain contours around the notch to micro-CT images. The finite element model was created with four-node plane stress elements and analyzed with ABAQUS (ABAQUS V6.3, ABAQUS, Inc.). Isotropic material properties were assigned to the bone tissue, using a Young's modulus of 18 GPa [22] and Poisson's ratio of 0.3. The models were analyzed with multiple levels of applied displacement to adjust the maximum principal strain around the notch tip.

RESULTS AND DISCUSSION

Micro-CT images of damaged specimens showed high intensity voxels within the bone tissue in regions ahead of the notch tip, as well as on free surfaces, propagating cracks and within vasculature (Figs. 3 and 4). Principle strain contours calculated by FEA exhibited a characteristic kidney shape of highest intensity ahead of the notch tip (Fig. 4c) which was consistent with the stained regions observed in micro-CT images (Figs. 3 and 4a). Stained regions ahead of the notch tip were not observed in unloaded control specimens (Fig. 3). Note, however, that some damage was likely induced during the preparation of notches. This damage was assumed to be similar between specimens assigned to each group.

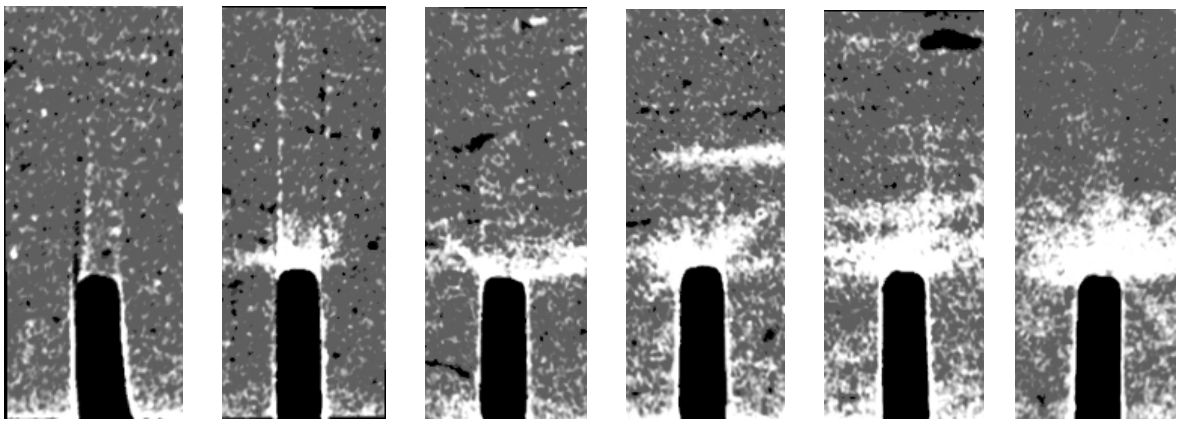

Figure 3. Representative two-dimensional micro-CT images of the unloaded control and specimens loaded to 10^5, $2{\cdot}10^5$, $3{\cdot}10^5$, $4{\cdot}10^5$ and $5{\cdot}10^5$ (from left to right) showing the stained region ahead of the notch. The width of each field is 1.2 mm.

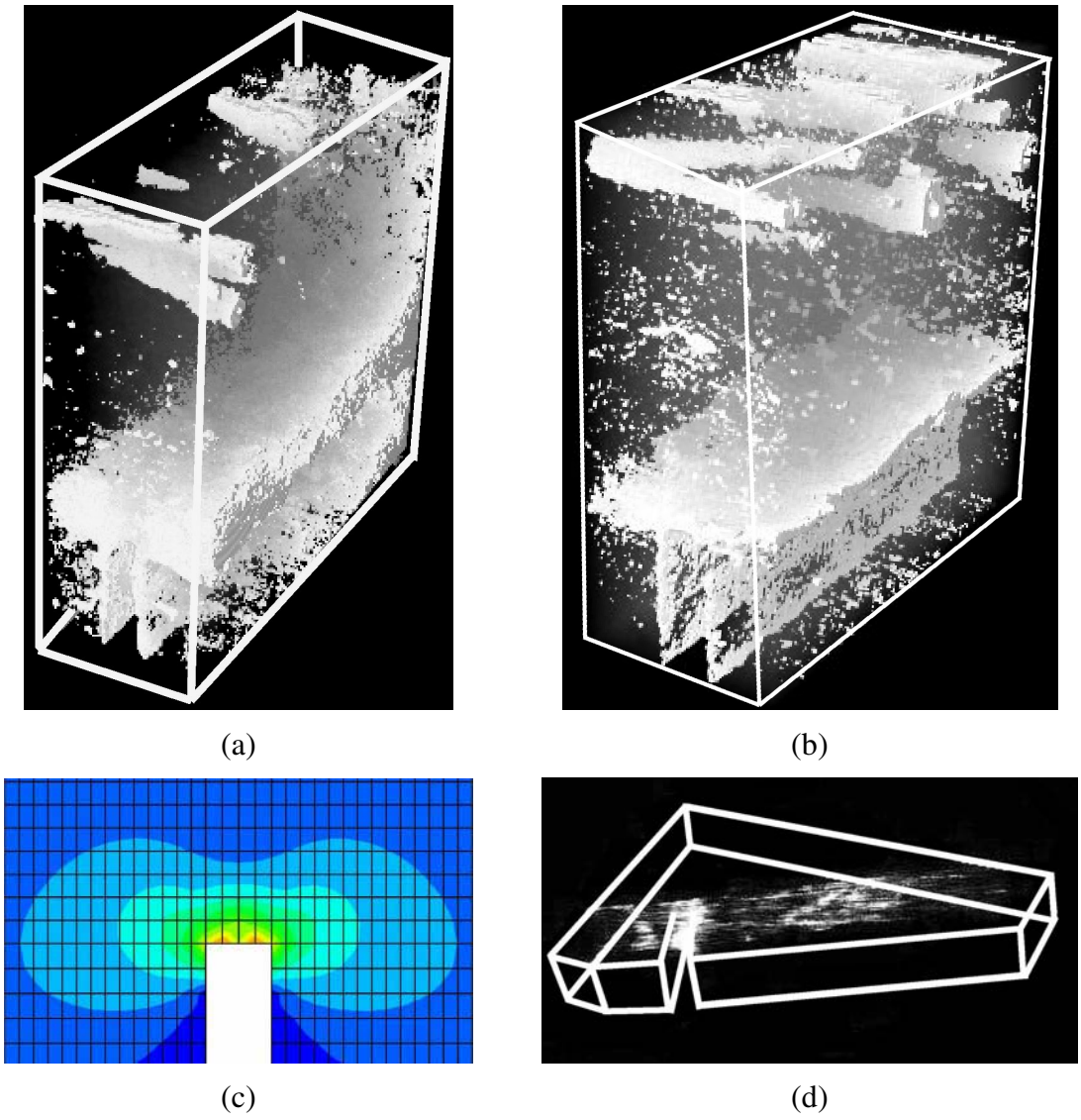

Figure 4. Three-dimensional micro-CT images reconstructed from transverse slices for specimens loaded to $5{\cdot}10^5$ cycles, showing (a) a specimen with a damaged region ahead of the notch and (b) a specimen with a macroscopic crack propagating from the notch tip. Note that $BaSO_4$ also stained the vasculature shown at the top of each image. (c) The shape of the damaged in region in (a) corresponded to principal strain contours calculated by FEA. (d) The propagating crack in (b) was shown by a micro-CT image reconstructed from longitudinal slices.

Staining ahead of the notch tip was much less prominent in specimens where a macroscopic crack propagated from the notch (Figs. 4b and 4d). Primary bovine cortical bone has a plexiform (or fibrolamellar) organization with packets of lamellar bone separated by less-organized woven bone [23]. The preparation of cortical bone beams in this study was such that interlamellar interfaces and most vasculature were oriented along the beam length. Therefore, cracks propagated along the beam length, normal to the notch (Figs. 4b and 4d, Fig. 5a). The presence of a propagating crack acted to release energy and inhibit further microdamage accumulation ahead of the notch tip. Therefore, decreased staining in specimens with propagating cracks was due to decreased damage accumulation.

BEI was used in order to observe microdamage and propagating cracks at higher resolution (Fig. 5a). Damaged tissue and propagating cracks exhibited a higher intensity due to the presence of precipitated $BaSO_4$. EDS verified that the intensity of bright voxels corresponded to the amount of staining (Fig. 5b). The highest level of elemental Ba and S was detected in propagating cracks. Lower levels of Ba and S were detected in tissue ahead of the notch that was damaged prior to crack initiation. No stain was detected in regions of tissue far away from the notch where minimal damage would be expected.

The amount of $BaSO_4$ stain was positively correlated to microdamage accumulation, both qualitatively and quantitatively. Micro-CT images showed that the amount of staining ahead of the notch tip increased with an increased number of loading cycles (Fig. 3). The amount of staining was measured from micro-CT image histograms by the ratio of the $BaSO_4$ integrated peak intensity to the overall integrated peak intensity, and was linearly and positively correlated with the number of loading cycles ($R^2 = 0.5$, $p < 0.0001$) (Fig. 6). Seven of the twenty-four total specimens were not included in the regression due to the presence of macroscopic propagating cracks which, as discussed above, inhibited microdamage accumulation ahead of the notch.

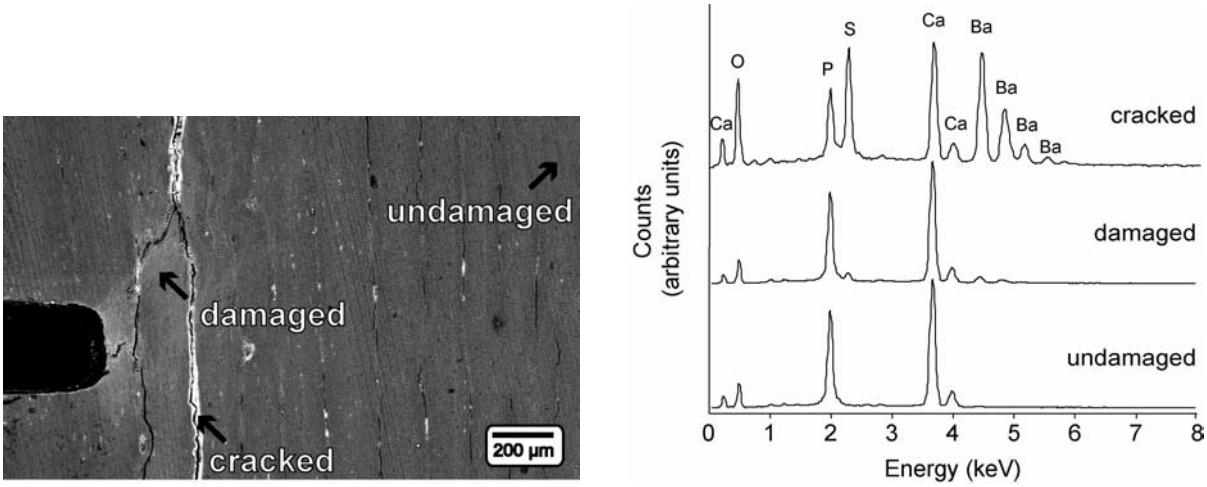

(a) (b)

Figure 5. (a) SEM micrograph using BEI of a cracked specimen loaded to 50,000 cycles and stained with $BaSO_4$. (b) The elemental composition measured at cracked, damaged and undamaged locations using EDS.

Figure 6. Linear regression of the ratio of $BaSO_4$ to overall integrated peak intensity with the number of loading cycles. Linear regression of the data yielded $y = 0.21 + 3.8 \cdot 10^{-7} \cdot x$ ($R^2 = 0.5$, $p < 0.0001$).

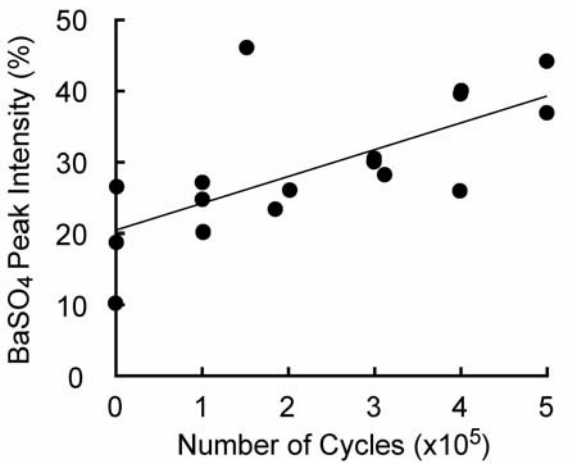

SUMMARY

$BaSO_4$ staining enabled micro-CT to image microdamage in bovine cortical bone three-dimensionally and nondestructively. The amount of staining was qualitatively and quantitatively correlated to microdamage accumulation. Microdamage accumulated ahead of a notch (stress concentration) until a macroscopic crack was initiated which limited further microdamage accumulation. Staining by $BaSO_4$ precipitation was nonspecific, including all void space such as vasculature and free surfaces. Therefore, a damage specific contrast agent with functional groups able to bind to calcium exposed on microcracks is under investigation.

ACKNOWLEDGEMENTS

This research was supported by the National Institutes of Health AR049598.

REFERENCES

1. W.S.S. Jee, in *Bone Mechanics Handbook*, edited by S. C. Cowin (CRC Press, Boca Raton, 2001) pp. 1.1-1.2.
2. D.B. Burr, M.R. Forwood, D.P. Fyhrie, R.B. Martin, M.B. Schaffler and C.H. Turner, *J Bone Miner Res*. **12**, 6-15 (1997).
3. R.B. Martin, *Calcif Tissue Int*. **73**, 101-107 (2003).
4. M.B. Schaffler, E.L. Radin and D.B. Burr, *Bone*. **10**, 207-214 (1989).
5. K.J. Jepsen and D.T. Davy, *J Biomechanics*. **30**, 891-894 (1997).
6. R.B. Martin and D.B. Burr, *J Biomechanics*. **15**, 137-139 (1982).
7. D.B. Burr, R.B. Martin, M.B. Schaffler and E.L. Radin, *J Biomechanics*. **18**, 189-200 (1985).
8. S. Mori and D.B. Burr, *Bone*. **14**, 103-109 (1993).
9. D.B. Burr and T. Stafford, *Clin Orthop Rel Res*. **260**, 305-308 (1990).
10. T.C. Lee, T.L. Arthur, L.J. Gibson and W.C. Hayes, *J Orthop Res*. **18**, 322-325 (2000).
11. F.J. O'Brien, D. Taylor and T.C. Lee, *J Biomechanics*. **35**, 523-526 (2002).
12. F.J. O'Brien, D. Taylor and T.C. Lee, *J Biomechanics*. **36**, 973-980 (2003).
13. M.B. Schaffler, W. Pitchford, K. Choi and J.M. Riddle, *Bone*. **15**, 483-488 (1994).
14. P. Zioupos and J.D. Currey, *J Biomechanics*. **27**, 993-5 (1994).
15. F.J. O'Brien, D. Taylor, G.R. Dickson, and T.C. Lee, *J Anat*. **197**, 413-420 (2000).
16. J. Li, M.A. Miller, G.D. Hutchins and D.B. Burr, *Trans Orthop Res Soc.* **30**, 33 (2005).
17. H. Leng, J.J. VanDersarl, G.L. Niebur and R.K. Roeder, *Trans Orthop Res Soc.* **30**, 665 (2005).
18. D.B. Masse, X. Wang, R.K. Roeder and G.L. Niebur, *Trans Orthop Res Soc*. **30**, 35 (2005).
19. R.K. Nalla, J.H. Kinney and R.O. Ritchie, *Nature Mater*. **2**, 164-168 (2003).
20. R.K. Nalla, J.J. Kruzic, J.H. Kinney and R.O. Ritchie, *Bone*. **35**, 1240-1246 (2004).
21. O.S. Sobelman, J.C. Gibeling, S.M. Stover, S.J. Hazelwood, O.C. Yeh, D.R. Shelton and R.B. Martin, *J Biomechanics*. **37**, 1295-1303 (2004).
22. D.T. Reilly and A.H. Burstein, *J Bone Joint Surg*. **56**, 1001-1022 (1974).
23. J.D. Currey, in *Bone Mechanics Handbook*, edited by S. C. Cowin (CRC Press, Boca Raton, 2001) pp. 19.1-19.4.